Title

The multiple absorption coefficient zonal method (MACZM), an efficient computational approach for the analysis of radiative heat transfer in multidimensional inhomogeneous nongray media

Journal

Numerical Heat Transfer Part B-Fundamentals, 49(2)

ISSN

1040-7790

Author

Yuen, W W

Publication Date

2006-02-01

Peer reviewed

The Multiple Absorption Coefficient Zonal Method (MACZM), an Efficient Computational Approach for the Analysis of Radiative Heat Transfer in Multi-Dimensional Inhomogeneous Non-gray Media

Walter W. Yuen
Department of Mechanical and Environmental Engineering
University of California at Santa Barbara
Santa Barbara, California, 93105

ABSTRACT

The formulation of a multiple absorption coefficient zonal method (MACZM) is presented. The concept of generic exchange factors (GEF) is introduced. Utilizing the GEF concept, MACZM is shown to be effective in simulating accurately the physics of radiative exchange in multi-dimensional inhomogeneous non-gray media. The method can be directly applied to a fine-grid finite-difference or finite-element computation. It is thus suitable for direction implementation in an existing CFD code for analysis of radiative heat transfer in practical engineering systems.

The feasibility of the method is demonstrated by calculating the radiative exchange between a high temperature (~3000 K) molten nuclear fuel (UO_2) and water (with a large variation in absorption coefficient from the visible to the infrared) in a highly 3-D and inhomogeneous environment simulating the premixing phase of a steam explosion.

NOMENCLATURE

a = absorption coefficient
A = area element
dA = differential area element
dV = differential volume element
D = length scale (grid size) of the discretization

F_{ggzz} = dimensionless volume-volume exchange factor, Eq. (11a)

F_{ggxz} = dimensionless volume-volume exchange factor, Eq. (11b)

F_{gsz} = dimensionless volume-surface exchange factor, Eq. (14a)

F_{gsx} = dimensionless volume-surface exchange factor, Eq. (14b)

$g_1 g_2$ = volume-volume exchange factor, Eq. (1)

$g_1 s_2$ = volume-surface exchange factor, Eq. (5)

L_c = characteristic lengths between two elements along the selected optical path

L_{mb} = mean beam length between two volume (area) elements, Eq. (16)

$\vec{n}$ = unit normal vector

n_x, n_y, n_z = dimensionless distance coordinate, Eq. (12)

r = distance between volume elements, Eq. (3)

s = distance, Eq. (4)

$s_1 s_2$ = surface-surface exchange factor, Eq. (6)

V = volume element

Q = heat transfer

T = temperature

x = coordinate

y = coordinate

z = coordinate

σ = Stefan Boltzmann constant

τ = optical thickness, Eq. (3)

subscripts

1,2 = label of volume (area) element

INTRODUCTION

The ability to assess the effect of radiation heat transfer in multi-dimensional inhomogeneous media is important in many engineering applications such as the analysis of practical combustion systems and the mixing of high temperature nuclear fuel (UO_2) with water in the safety consideration of nuclear reactors. Over the years, many different solution techniques with various level of complexity (e.g. the differential (PN) method [1, 2], the multi-flux or the discrete ordinate methods [3-7]), the discrete transfer method [8-11], the finite volume method [12-15], the finite element method [16, 17], the Monte Carlo method [18-21] and the zonal method [22-24]) have been developed to provide a quantitative assessment of the radiation effect. While these techniques all have some degree of success in demonstrating certain effects of the radiation heat transfer, particularly in simplified idealized conditions (e.g. 1D or 2D gray homogenous medium), none of these techniques have been developed sufficiently so that it can be used robustly and accurately in the design of practical engineering systems.

Indeed, the lack of a computationally efficient and accurate approach has been a major difficulty limiting engineers and designers from addressing many important engineering issues accounting for the effect of thermal radiation. For example, in the analysis of steam explosion for a reactor safety consideration, it is important for account for the radiative exchange between hot molten material (e.g. UO_2) and water. The absorption coefficient for water is plotted together with the blackbody emissive power at 3052 K (the expected temperature of molten UO_2 in a nuclear accident scenario) in Figure 1. The radiative exchange between water and UO_2 must account for the highly nongray and rapidly increasing (by more than two order of magnitude) characteristic of the absorption coefficient of water. The multi-dimensional and inhomogeneous aspect of the "premixing" process are illustrated by Figure 2. In this particular scenario, molten UO_2 is released from the top into a cylindrical vessel with an annular overflow chamber as shown in the figure. Even with highly subcooled water (say, 20 C at 1 atm), voiding occurs quickly leading to a complex two phase mixture surrounding the hot molten UO_2. The radiative heat transfer between the hot molten UO_2 and the surrounding water is a key mechanism controlling the boiling process. The boiling process, on the other hand, depends on the radiative heat transfer and thus the amount of liquid water surrounding the hot molten material. An accurate assessment of this interaction is key to the understanding of this "premixing" process

and ultimately to the resolution of the critical issue of steam explosion in the consideration of reactor safety.

Over the years, the zonal method has been shown to be an effective approach to account for the multi-dimensional aspect of radiative heat transfer in homogeneous and isothermal media [22,23]. This method was later extended for application to inhomogeneous and non-isothermal media with the concept of "generic" exchange factors (GEF) [24]. The underlying principle of the extended zonal method is that if a set of generic exchange factors with standard geometry is tabulated, the radiative exchange between an emitting element and an absorbing element of arbitrary geometry can be generated by superposition. The inhomogeneous nature can be accounted for by using the appropriate average absorption coefficient in the evaluation of the generic exchange factor. As grid size decreases, it is expected that the accuracy of the superposition will increase. The error of using a single average absorption to account for the absorption characteristics of the intervening medium will also decrease.

While the extended zonal method was effective in accounting for the effect of an inhomogeneous medium in some problems [24], the accuracy of the approach for general application is limited. Specifically, by using a set of GEF which depends on only a single average absorption coefficient, the method do not simulate correctly the physics of radiative exchange between two volume elements which depends generally on at least three characteristic absorption coefficients (namely, the absorption coefficient of the emitting element, the absorption coefficient of the absorbing element and the average absorption coefficient of the intervening medium). A reduction in grid size alone cannot address this fundamental limitation.

In addition, the concept of a single average absorption coefficient for the intervening medium is also insufficient, particularly in an environment where there is a large discontinuity of the absorption coefficient in areas around either the absorbing or emitting elements. For example, consider the radiative exchange between a radiating cubical water element V_1 and an absorbing cubical water element V_2 as shown in Figure 3. The absorbing element V_2 is an element situated at a liquid/vapor phase boundary. It is adjacent to another element of liquid water on one side while surrounded by a medium which is effectively optically transparent. As shown in the same figure, there are two possible optical paths, indicated as S_1 and S_2, over which the average absorption coefficient can be evaluated. For the physical dimensions as shown in the figure, the average absorption coefficient evaluated along the optical path S_2 increases from 6.38

1/cm to 306 1/cm as the wavelength increases from 0.95 μm to 3.27 μm while the average absorption coefficient evaluated along the optical path S_1 remains effectively at zero (ignoring the very small absorption by water vapor). It would be difficult to evaluate the radiative exchange between the two elements V_1 and V_2 accurately using a single exchange factor based on a single average absorption coefficient for the intervening medium. This large discrepancy in the average absorption coefficient of the two optical paths remains even in the limit of small grid size.

The objective of the present work is to present the mathematical formulation of a multiple absorption coefficient zonal method (MACZM) which is mathematically consistent with the physics of radiative absorption. The method will be shown to be efficient and accurate in the simulation of radiative heat transfer in inhomogeneous media. A set of "three absorption coefficient" volume-volume exchange factors and "two absorption coefficient" volume-surface exchange factors are tabulated for rectangular elements. The generic exchange factor (GEF) concept is expanded to a two-component formulation to account for the possible large variation of absorption coefficient in regions surrounding the absorbing or emitting elements. Based these two-component generic exchange factors, the multi-dimensional and non-gray effect in any discretized domain can be evaluated accurately and efficiently by superposition. The accuracy of the superposition procedure is demonstrated by comparison with results generated by direct numerical integration. The characteristics of radiative exchange in a highly multi-dimensional, inhomogeneous and non-gray media such as those existed in the premixing phase of a steam explosion (as shown in Figure 2) are presented to illustrate the feasibility of the approach.

MATHEMATICAL FORMULATION

General Formulation

The basis of the zonal method [22] is the concept of exchange factor. Mathematically, the exchange factor between two discrete volumes, V_1 and V_2, in a radiating environment is

$$g_1 g_2 = \int_{V_1}\int_{V_2} \frac{a_1 a_2 e^{-\tau} dV_1 dV_2}{\pi r^2} \qquad (1)$$

where

$$r = \left[\left(x_1 - x_2 \right)^2 + \left(y_1 - y_2 \right)^2 + \left(z_1 - z_2 \right)^2 \right]^{1/2} \tag{2}$$

τ is the optical thickness between the two differential volume elements, dV_1 and dV_2, given by

$$\tau = \int_{\vec{r}_1}^{\vec{r}_2} a(s)\, ds \tag{3}$$

with a being the absorption coefficient and

$$s = \left| \vec{r} - \vec{r}_1 \right| \tag{4}$$

The integration in Eq. (3) is performed along a straight line of sight from $\vec{r}_1$ to $\vec{r}_2$.

In a similar manner, the exchange factor between a volume element V_1 and a surface element A_2 and that between two area elements A_1 and A_2 are given, respectively, by

$$g_1 s_2 = \int_{V_1} \int_{A_2} \frac{a_1 e^{-\tau} \left| \vec{n}_2 \cdot \vec{r} \right| dV_1 dA_2}{\pi r^3} \tag{5}$$

$$s_1 s_2 = \int_{A_1} \int_{A_2} \frac{e^{-\tau} \left| \vec{n}_1 \cdot \vec{r} \right| \left| \vec{n}_2 \cdot \vec{r} \right| dA_1 dA_2}{\pi r^4} \tag{6}$$

where $\vec{n}_1$ and $\vec{n}_2$ are unit normal vectors of area elements dA_1 and dA_2.

It should be noted that Eqs. (1), (5) and (6) are applicable for general inhomogeneous non-scattering media in which the absorption coefficient is a function of position. Physically, the exchange factor can be interpreted as the fraction of energy radiated from one volume (or area) and absorbed by a second volume (or area). Specifically, for a volume V_1 with uniform temperature T_1, the absorption by a second volume V_2 of radiation emitted by V_1 is given by

$$Q_{V_1 \to V_2} = \sigma T_1^4 g_1 g_2 \tag{7}$$

and the absorption by a black surface A_2 of radiation emitted by V_1 is given by

$$Q_{V_1 \to A_2} = \sigma T_1^4 g_1 s_2 \tag{8}$$

Similarly, for a black surface A_1 with uniform temperature T_1, the absorption by a volume V_2 of radiation emitted by A_1 is given by

$$Q_{A_1 \to V_2} = \sigma T_1^4 s_1 g_2 \tag{9a}$$

where, by reciprocity,

$$s_1 g_2 = g_2 s_1 \tag{9b}$$

Finally, the absorption by a black surface A_2 of radiation emitted by A_1 is given by

$$Q_{A_1 \to A_2} = \sigma T_1^4 s_1 s_2 \qquad (10)$$

The Discretization

The evaluation of Eqs. (7) to (10) in a general transient calculation in which the spatial distribution of the absorption coefficient is changing (for example, due to the change in the spatial distribution of hot materials and void fraction during the "premixing" process as shown in Figure 2) is too time consuming even with fast computers. Anticipating that all calculations will be generally done in a discretized computational domain, it is useful to develop a set of "generic" exchange factors (GEF) which will be applicable for all calculations.

Specifically, consider the geometry as shown in Figure 4. Assuming that the absorption coefficient within the two discrete volumes (a_1 and a_2) are constant, MACZM introduces two partial exchange factors, $(g_1 g_2)_{zz}$ and $(g_1 g_2)_{xz}$ to characterize the radiative exchange between the two volumes. The parallel exchange factor $(g_1 g_2)_{zz}$ represents the radiative exchange between the two volume consisting only of those energy rays which pass through the top surface of V_1 ($z = z_1 + D$) and the bottom surface of V_2 ($z = z_1 + n_z D$). The transverse exchange factor $(g_1 g_2)_{xz}$, on the other hand, represents the radiative exchange between the two volume consisting only of those energy rays which pass through the "x-direction" side surface of V_1 ($x = x_1 + D$) and the bottom surface of V_2 ($z = z_1 + n_z D$). Assuming that the absorption coefficient of the intervening medium is constant (but different for the two partial exchange factors), the two partial exchange factors can be expressed in the following dimensionless form

$$\frac{(g_1 g_2)_{zz}}{D^2} = F_{ggzz}\left(a_1 D, a_2 D, a_{m,zz} D, n_x, n_y, n_z\right) \qquad (11a)$$

$$\frac{(g_1 g_2)_{xz}}{D^2} = F_{ggxz}\left(a_1 D, a_2 D, a_{m,xz} D, n_x, n_y, n_z\right) \qquad (11b)$$

with

$$n_x = \frac{x_2 - x_1}{D}, \quad n_y = \frac{y_2 - y_1}{D}, \quad n_z = \frac{z_2 - z_1}{D} \tag{12}$$

The two functions $F_{ggzz}\left(a_1 D, a_2 D, a_{m,zz} D, n_x, n_y, n_z\right)$ and $F_{ggxz}\left(a_1 D, a_2 D, a_{m,xz} D, n_x, n_y, n_z\right)$ are dimensionless functions of the three optical thicknesses $\left(a_1 D, a_2 D, a_{m,zz} D \text{ or } a_{m,xz} D\right)$ and the dimensionless separation between the two volume elements $\left(n_x, n_y, n_z\right)$. For a rectangular discretization with constant grid size (dx = dy = dz = D), these dimensionless distances only take on discretized value, i.e. $n_x, n_y, n_z = 0, 1, 2 \cdots$. The two dimensionless functions tabulated at different optical thicknesses $\left(a_1 D, a_2 D, a_{m,zz} D \text{ or } a_{m,xz} D\right)$ and discretized values of $\left(n_x, n_y, n_z\right)$ constitutes two sets of "generic" exchange factor (GEF) which will be applicable for all calculations with uniform grid size. The intervening absorption coefficient $a_{m,zz}$ is the average of the absorption coefficient taken along a line of sight directed from the center of the top area element of V_1 ($z = z_1$) to the center of the bottom surface of V_2 ($z = z_1 + n_z D$). Similarly, the intervening absorption coefficient $a_{m,xz}$ is the average of the absorption coefficient taken along a line of sight directed from the center of the "x-direction" side area element of V_1 ($x = x_1 + D$) to the center of the bottom surface of V_2 ($z = z_1 + n_z D$).

Mathematically, the exchange factor between the two cubical volumes can be generated from Eqs. (11a) and (11b) by superposition as

$$
\begin{aligned}
\frac{g_1 g_2}{D^2} &= F_{ggzz}\left(a_1 D, a_2 D, a_{m,zz} D, n_x, n_y, n_z\right) \\
&+ F_{ggxz}\left(a_1 D, a_2 D, a_{m,xz} D, n_x, n_y, n_z\right) \\
&+ F_{ggxz}\left(a_1 D, a_2 D, a_{m,yz} D, n_y, n_x, n_z\right) \\
&+ F_{ggzz}\left(a_1 D, a_2 D, a_{m,yy} D, n_z, n_x, n_y\right) \\
&+ F_{ggxz}\left(a_1 D, a_2 D, a_{m,zy} D, n_z, n_x, n_y\right) \\
&+ F_{ggxz}\left(a_1 D, a_2 D, a_{m,xy} D, n_x, n_z, n_y\right) \\
&+ F_{ggzz}\left(a_1 D, a_2 D, a_{m,xx} D, n_y, n_z, n_x\right) \\
&+ F_{ggxz}\left(a_1 D, a_2 D, a_{m,yx} D, n_y, n_z, n_x\right) \\
&+ F_{ggxz}\left(a_1 D, a_2 D, a_{m,zx} D, n_z, n_y, n_x\right)
\end{aligned}
\qquad (13)
$$

Eq. (13), together with the tabulated values of the two GEF's, $F_{ggzz}\left(a_1 D, a_2 D, a_{m,zz} D, n_x, n_y, n_z\right)$ and $F_{ggxz}\left(a_1 D, a_2 D, a_{m,xz} D, n_x, n_y, n_z\right)$, contain all the essential physics needed to characterize the radiative exchange between the two elements. These two factors account for the absorption characteristics of the absorbing and emitting element $\left(a_1 D, a_2 D\right)$. By using different average absorption coefficients $\left(a_{m,pq} D,\ p,q = x,y,z\right)$ for the intervening medium, they accounts for not only the absorption characteristics of the intervening medium, but also and the variation of absorption characteristics in the neighborhood of the absorbing and emitting elements (such as the situation as shown in Figure 3).

The exchange factor $g_1 s_2$ can be similarly expressed in a dimensionless form. Using the geometry as shown in Figure 5, two partial exchange factors, $\left(g_1 s_2\right)_z$ and $\left(g_1 s_2\right)_x$, are introduced. Physically, the parallel exchange factor $\left(g_1 s_2\right)_z$ represents the radiative exchange between V_1 and A_2 consisting only of those energy rays which pass through the top surface of V_1 ($z = z_1 + D$). The transverse factor $\left(g_1 s_2\right)_x$, on the other hand, represents the radiative exchange between V_1 and A_2 consisting only of those energy rays which pass through the "x-direction" side surface of V_1 ($x = x_1 + D$). Assuming that the absorption coefficient of the intervening medium is constant (but different for the two partial exchange factors), the two partial exchange factors can be expressed in the following dimensionless form

$$\frac{(g_1 s_2)_z}{D^2} = F_{gsz}\left(a_1 D, a_{m,z} D, n_x, n_y, n_z\right) \tag{14a}$$

$$\frac{(g_1 s_2)_x}{D^2} = F_{gsx}\left(a_1 D, a_{m,x} D, n_x, n_y, n_z\right) \tag{14b}$$

Note that in Figure 5, the area A_2 is assumed to be parallel to the x-y plane. For general application, this does not represent a loss of generality since a discretized area is always parallel to one of the face of the discretized volume in a rectangular coordinate system with equal grid size. The two average absorption coefficients are taken along the two line of sights directed toward the center of the receiving plane, from the top area element ($z = z_1 + D$) and x-direction side area element ($x = x_1 + D$) respectively. Similar to Eq. (13), the exchange factor between V_1 and A_2 can be generated by superposition as

$$\begin{aligned}\frac{g_1 s_2}{D^2} &= F_{gsz}\left(a_1 D, a_{m,z} D, n_x, n_y, n_z\right) \\ &+ F_{gsx}\left(a_1 D, a_{m,x} D, n_x, n_y, n_z\right) \\ &+ F_{gsx}\left(a_1 D, a_{m,y} D, n_y, n_x, n_z\right)\end{aligned} \tag{15}$$

The exchange factor $s_1 s_2$ is a function of only one average absorption coefficient for the intervening medium (a_m). Its formulation and mathematical behavior have already been presented and discussed in the earlier work [24] and will not be repeated here.

The "Generic" Exchange Factor (GEF) and its Properties

Numerical data for the "generic" exchange factors are tabulated and they are presented in detail elsewhere [26]. For a practical calculation, these factors can serve as a "look-up" table based on which the radiative exchange can be computed accurately and efficiently by superposition.

Since GEF are functions only of optical thicknesses and geometric orientation, the accuracy of the superposition procedure is generally insensitive to the physical dimension D (i.e. the grid size). As an illustration, the radiative exchange between a volume element and area

element as shown in Figure 6 is considered. The superposition solutions are generated by subdividing the volume and area into cubical volume and area elements with dimension Δ. A comparison between the superposition solution and that generated by direct numerical integration is shown in Table 1. For the two volume elements as shown in Figure 7, a similar comparison is shown in Table 2. In both cases, the accuracy of the superposition results appears to be somewhat insensitive to the dimension Δ. The slight discrepancy can be attributed to the error in the interpolation of the "look-up" table over discrete optical thicknesses. The numerical data presented in the two tables, for example, are generated with a set of GEF tabulated for $a_1D, a_2D, a_mL_c =$ 0, 0.11, 0.16, 0.22, 0.36, 0.44, 0.51 where L_c is the characteristic distance between the emitting and absorbing elements. This set of optical thickness corresponds approximately to the value for which the transmissivity ($\tau = e^{-a_1D}, e^{-a_2D}$ or $e^{-a_mL_c}$) is 1.0, 0.9, 0.8, 0.7, 0.6, 0.5 and 0.4 respectively. The accuracy can be readily improved by tabulating GEF at more optical thicknesses. Note that for practical application, the grid size is important only in determining how well the rectangular discretization simulates the actual geometry. When the geometry is simulated accurately, the accuracy of MACZM depends only on the number of discrete data points used in the GEF table.

APPLICATION

MACZM is applied to analyze the effect of radiation on the mixing of hot molten fuel with water. The formulation of the full numerical model for the simulation of the mixing behavior is presented elsewhere [25]. For simplicity, the radiative absorption of steam is neglected in the calculation. The detailed analysis and results will be presented in future publications. In the present work, the predicted radiative heat transfer distribution is presented to illustrate the effectiveness of MACZM.

Because of the large variation of the absorption coefficient of water over the wavelength of interest as shown in Figure 1, a three-band approach is used to capture the difference in radiative energy distribution in the different wavelength region. The step wise approximation used for the absorption coefficient of water is shown in Figure 8. The absorption coefficients of the three bands correspond to the absorption coefficient of three characteristic wavelengths 0.4915 μm, 0.9495 μm and 3.277 μm respectively. The middle wavelength (0.9495 μm) is the

wavelength at which the blackbody emissive power at the molten fuel temperature (3052 K) is a maximum. The fractions of energy radiated by the molten fuel (at 3052 K) for the three bands are 0.125, 0.647 and 0.228 respectively. Using a grid size of 10 cm (with the inner vessel diameter of 70 cm), the rate of energy absorption by water predicted for three different times during the premixing transient are shown in Figures 9a, 9b and 9c. It can be readily observed that the distribution of water energy absorption varies significantly among the three bands. In the first band at which water is optically transparent, the radiation penetrates a significant distance away from the radiating molten fuel. This accounts for the "red hot" visual appearance commonly observed in the interaction of high temperature molten fuel and water. The first band, however, accounts only for 12.5% of the total energy radiated from the fuel. For the remaining energy, the water absorption coefficient is high and the water absorption is highly localized in the region surrounding the fuel. The localized absorption appears to dominate the boiling process as the second and third band account for more than 80% of the radiative emission. MACZM captures both the transient and spatial distribution of the radiative absorption distribution accurately and efficiently.

Because of the large variation of the water absorption coefficient over wavelength and the large values of the water absorption coefficient in the long wavelength region, a larger number of band and smaller grid size are needed to simulate accurately the effect of radiation on the premixing process. This effort is currently underway and results will be presented in future publications.

CONCLUSION

The formulation of a multiple absorption coefficient zonal method (MACZM) is presented. Four "generic" exchange factors (GEF) are shown to be accurate and effective in simulating the radiative exchange. Numerical values these GEF's are tabulated and their mathematical behavior is described.

MACZM is shown to be effective in capturing the physics of radiative heat transfer in a multi-dimensional inhomogeneous three phase mixture (molten fuel, liquid and vapor) generated in the premixing phase of a steam explosion.

REFERENCES

1. A. Ratzel and J. R. Howell, “Two-Dimensional Energy Transfer in Radiatively Participating Media with Conduction by the P-N Approximation”, Proceeding of the 1982 International Heat Transfer Conference, Vol. 2 (1982), pp. 535-450.
2. Y. Bayazitoglu and J. Higenyi, “The Higher-Order Differential Equations of Radiative Heat Transfer, the P-3 Approximation”, AIAA Journal, Vol. 7, No. 4 (1979), pp. 424-431.
3. S. Chandrasekhar, “Radiative Transfer”, Dover, New York, 1960.
4. K. D. Lathrop, “Use of Discrete Ordinate Methods for Photon Transport Problem”, Nuclear Science and Engineering, Vol. 24 (1966), pp. 381-388.
5. W. A. Fiveland, “Discrete Ordinate Method for Radiative Transfer in Isotropically and Anisotropically Scattering Media”, Journal of Heat Transfer, Vol. 109, No. 3 (1987), pp. 809-812.
6. N. Selcuk and. I. Ayranci, “The Method of Lines Solution of the Discrete Ordinate Method for Radiative Transfer in Enclosures Containing Scattering Media”, Numerical Heat Transfer, Part B, Fundamentals, Vol. 43, No. 2 (2003), pp. 179-201.
7. G. Krisnamoorthy, R. Rawat and P. J. Smith, “Parallel Computations of Radiative Heat Transfer Using the Discrete Ordinate Method”, Numerical Heat Transer, Part B, Fundamentals, Vol. 47, No. 1 (2005), pp. 19-38.
8. F. C. Lockwood and N. G. Shah, “A New Radiation Solution Method for Incorporation in General Combustion Procedures”, The 18th International Symposium on Combustion, the Combustion Institute (1981), pp. 1405-1414.
9. P. S. Cumber, “Improvement to the Discrete Transfer Method for Calculating Radiative Heat Transfer”, International Journal of Heat and Mass Transfer, Vol. 38, No. 12 (1995), pp. 2251-2258.
10. J. Liu, S. J. Zhang and Y. S. Chen, “An Improved Discrete Transfer Method for 3-D Surface Radiation Calculation”, Numerical heat Transfer, Part B, Fundamentals, Vol. 42, No. 3 (2002), pp. 203-214.
11. S. C. Mishra, P. Talukdar, D. Trimis and F. Durst, “Effect of Angular Quadrature Schemes on the Computational Efficiency of the Discrete Transfer Method for Solving Radiative Heat Transfer Problems with Pariticpating Medium”, Numerical Heat Transfer, Part B, Fundamentals, Vol. 46, No. 5 (2004), pp. 463-478.

12. J. Y. Murthy and S. R. Mathur, “Finite Volume Method for Radiative Heat Transfer Using Unstructured Meshes”, Journal of Thermophysics and Heat Transfer, Vol. 12, No. 3 (1998), pp. 313-321.
13. S. H. Kim and K. Y. Huh, “Assessment of the Finite-Volume Method and the Discrete Ordinate Method for Radiative Heat Transfer in a Three-Dimensional Rectangular Enclosure”, Numerical Heat Transfer, Part B, Fundamentals, Vol. 35, No. 1 (1999), pp. 85-112.
14. S. H. Kim and K. Y. Huh, “A New Angular Discretization Scheme of the Finite Volume Method for 3-D Radiative Heat Transfer in Absorbing, Emitting and Anisotropically Scattering Media”, International Journal of Heat and Mass Transfer, Vol. 43, No. 7 (2000), pp. 1233-1242.
15. G. D. Raithby, “Discussion of the Finite-Volume Method for Radiation, and its Application Using 3D Unstructured Meshes”, Numerical Heat transfer, Part B, Fundamentals, Vol. 35, No. 4 (1999), pp. 389-405.
16. M. M. Razzaque, D. E. Klein and J. R. Howell, “Finite Element Solution of Radiative Heat Transfer in a Two-Dimensional Rectangular Enclosure with Gray Participating Media”, Journal of Heat Transfer, Vol. 105, No. 4 (1983), pp. 933-934.
17. M. L. Nice, “Application of Finite Element Method to Heat Transfer in a Participating Medium”, Numerical Properties and Methodologies in Heat Transfer, T. M. Shih (Ed.), Hemisphere, Washing D.C. (1983), pp. 497-514.
18. J. R. Howell, “The Monte Carlo Method in Radiative Heat Transfer”, Journal of Heat Transfer, Vol. 120, No. 3 (1998), pp. 547-560.
19. D. V. Walters and R. O. Buckius, “Monte Carlo Method for Radiative Heat Transfer in Scattering Media”, Annual Review of Heat Transfer, C. L. Tien (Ed.), CRC Press, Boca Raton (1994), pp. 131-176.
20. M. F. Modest, “Monte Carlo Method Applied to Gases with Spectral Line Structure”, Numerical Heat Transfer, Part B, Fundamentals, Vol. 22, No. 3 (1992), pp. 273-284.
21. S. Mazumder and A. Kersch, “A Fast Monte Carlo Scheme for Thermal Radiation in Semiconductor Processing Applications”, Numerical Heat Transfer, Part B, Fundamentals, Vol. 37, No. 2 (2000), pp. 185-199.
22. H. C. Hottel and A. F. Sarofim, “Radiative Transfer”, McGraw Hill, New York, 1967.

23. J. J. Nobel, “The Zonal Method: Explicit Matrix Relations for Total Exchange Areas”, International Journal of Heat and Mass Transfer, Vol. 18, No. 2 (1975), pp. 261-269.
24. W. W. Yuen and E. E. Takara, “The Zonal Method, a Practical Solution Method for Radiative Transfer in Non-Isothermal Inhomogeneous Media”, Annual Review of Heat Transfer, Vol. 8 (1997), pp. 153-215
25. W. W. Yuen, T. G. Theofanous and S. Angelini, “The Verification Basis of the PM-ALPHA Code", Nuclear Engineering and Design, Vol. 189 (1999), pp. 103-138.
26. W. W. Yuen, “Numerical Data for the General Exchange Factor used in the Multiple Absorption Coefficient Zonal Method (MACZM)”, UCSB Report 2005-1, 2005.

m	a_1D	a_mD	Δ/D	$g_1s_2(a_1D, a_mD, 0, 0, m)$
1	0.1	0.1, 0.3, 0.5, 1.0	numerical	0.109e-1, 0.879e-2, 0.709e-2, 0.415e-2
			1/2	0.109e-1, 0.880e-2, 0.711e-2, 0.418e-2
			1/3	0.109e-1, 0.879e-2, 0.711e-2, 0.417e-2
			1/4	0.109e-1, 0.879e-2, 0.710e-2, 0.417e-2
1	1.0	0.1, 0.3, 0.5, 1.0	numerical	0.770e-1, 0.621e-1, 0.500e-1, 0.292e-1
			1/2	0.764e-1, 0.617e-1, 0.498e-1, 0.292e-1
			1/3	0.765e-1, 0.617e-1, 0.498e-1, 0.292e-1
			1/4	0.766e-1, 0.618e-1, 0.499e-1, 0.292e-1
2	0.1	0.1, 0.3, 0.5, 1.0	numerical	0.381e-2, 0.252e-2, 0.167e-2, 0.600e-3
			1/2	0.381e-2, 0.253e-2, 0.168e-2, 0.603e-3
			1/3	0.380e-2, 0.252e-2, 0.167e-2, 0.601e-3
2	1.0	0.1, 0.3, 0.5, 1.0	numerical	0.265e-1, 0.176e-1, 0.117e-1, 0.417e-2
			1/2	0.264e-1, 0.175e-1, 0.116e-1, 0.417e-2
			1/3	0.264e-1, 0.175e-1, 0.116e-1, 0.416e-2

Table 1: Comparison between the exchange factor generated by direct numerical integration and those generated by superposition of GEF for the geometry of Figure 6. (Δ is the length scale of the element used in the GEF superposition).

m_x, m_z	a_1D	a_mD	a_2D	Δ/D	g_1g_2 (a_1D, a_2D, a_mD, m_x, 0, m_z)
0, 0	= a_2D	N/A	0.1, 0.3, 0.5	numerical	0.183e-1, 0.153, 0.383
				1/2	0.194e-1, 0.148, 0.391
				1/3	0.175e-1, 0.149, 0.384
				1/4	0.175e-1, 0.155, 0.386
0, 1	0.1	N/A	0.1, 0.3, 0.5	numerical	0.351e-2, 0.973e-2, 0.150e-1
				1/2	0.351e-2, 0.973e-2, 0.150e-1
				1/3	0.352e-2, 0.974e-2, 0.151e-1
				1/4	0.352e-2, 0.976e-2, 0.151e-1
0, 1	0.5	N/A	0.1, 0.3, 0.5	numerical	0.150e-1, 0.417e-1, 0.644e-1
				1/2	0.150e-1, 0.417e-1, 0.644e-1
				1/3	0.151e-1, 0.417e-1, 0.645e-1
				1/4	0.151e-1, 0.418e-1, 0.646e-1
1, 1	0.1	0.0	0.1, 0.3, 0.5	numerical	0.164e-2, 0.451e-2, 0.692e-2
				1/2	0.164e-2, 0.450e-2, 0.689e-2
				1/3	0.164e-2, 0.451e-2, 0.690e-2
				1/4	0.165e-2, 0.452e-2, 0.692e-2
1, 1	0.1	0.5	0.1, 0.3, 0.5	numerical	0.138e-2, 0.379e-2, 0.580e-2
				1/2	0.139e-2, 0.381e-2, 0.582e-2
				1/3	0.140e-2, 0.383e-2, 0.585e-2
				1/4	0.140e-2, 0.384e-2, 0.587e02
1, 1	0.5	0.0	0.1, 0.3, 0.5	numerical	0.692e-2, 0.191e-1, 0.292e-1
				1/2	0.688e-2, 0.189e-1, 0.290e-1
				1/3	0.698e-2, 0.189e-1, 0.290e-1
				1/4	0.691e-2, 0.190e-1, 0.291e-1
1, 1	0.5	0.5	0.1, 0.3, 0.5	numerical	0.580e-2, 0.159e-1, 0.244e-1
				1/2	0.582e-2, 0.160e-1, 0.244e-1
				1/3	0.584e-2, 0.162e-1, 0.245e-1
				1/4	0.586e-2, 0.161e-1, 0.246e-1

Table 2: Comparison between the exchange factor generated by direct numerical integration and those generated by superposition of GEF for the geometry of Figure 7. (Δ is the length scale of the element used in the GEF superposition).

Figure Captions:

Figure 1: The absorption coefficient of water and the blackbody emissive power at 3052 K.

Figure 2: The distribution of molten UO_2 (left, with the black dot representing the "fuel" as lagrangian particles) and the void fraction distribution of water (right) during a premixing process.

Figure 3: Example geometry highlighting the difference in "average absorption coefficient" for different optical path.

Figure 4: Geometry and coordinate system used in the definition of the $g_1 g_2$ GEF.

Figure 5: Geometry and coordinate system used in the definition of the $g_1 s_2$ GEF.

Figure 6: Geometry and coordinate system used in the illustration of the accuracy of the superposition procedure for the evaluation of the exchange factor $g_1 s_2$.

Figure 7: Geometry and coordinate system used in the illustration of the accuracy of the superposition procedure for the evaluation of the exchange factor $g_1 g_2$.

Figure 8: The 3-band approximation of the water absorption coefficient used in the premixing calculation.

Figure 9a: The distribution of radiative absorption by water in the three absorption band (the right three figures) at 0.6 s after the initial pour predicted by the premixing calculation. The first figure on the left represents the distribution of the molten fuel (the black dots are the lagrangian particles representing fuel) and the second figure represents the void fraction distribution.

Figure 9b: The distribution of radiative absorption by water in the three absorption band (the right three figures) at 0.8 s after the initial pour predicted by the premixing calculation. The first figure on the left represents the distribution of the molten fuel (the black dots are the lagrangian particles representing fuel) and the second figure represents the void fraction distribution.

Figure 9c: The distribution of radiative absorption by water in the three absorption band (the right three figures) at 1.0 s after the initial pour predicted by the premixing calculation. The first figure on the left represents the distribution of the molten fuel (the black dots are the lagrangian particles representing fuel) and the second figure represents the void fraction distribution.

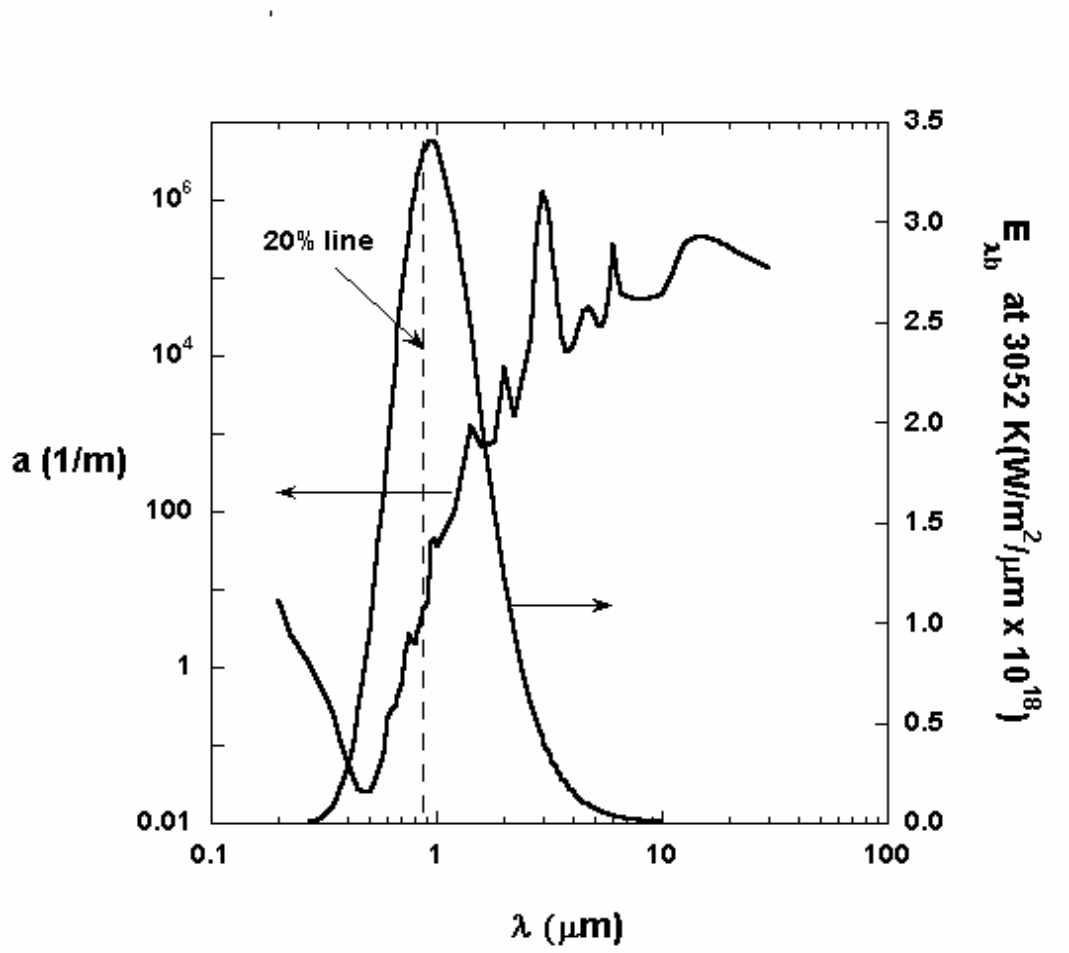

Figure 1: The absorption coefficient of water and the blackbody emissive power at 3052 K.

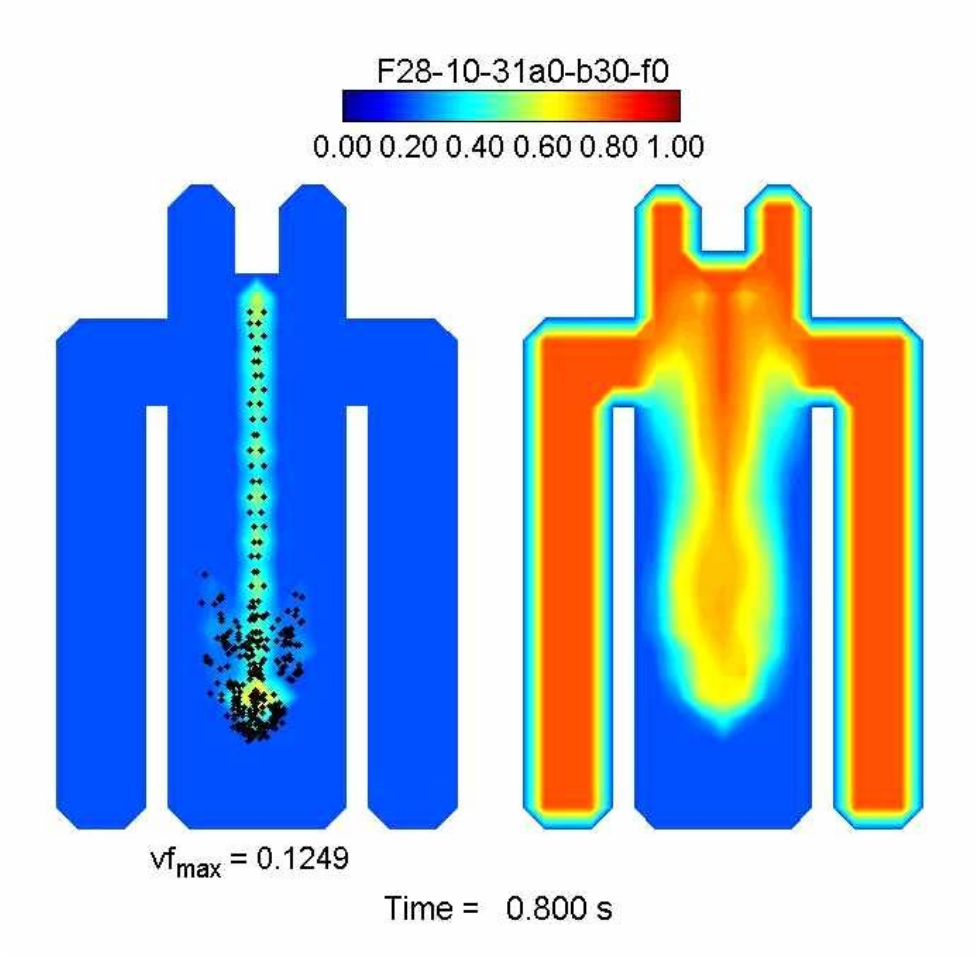

Figure 2: The distribution of molten UO_2 (left, with the black dot representing the "fuel" as lagrangian particles) and the void fraction distribution of water (right) during a premixing process.

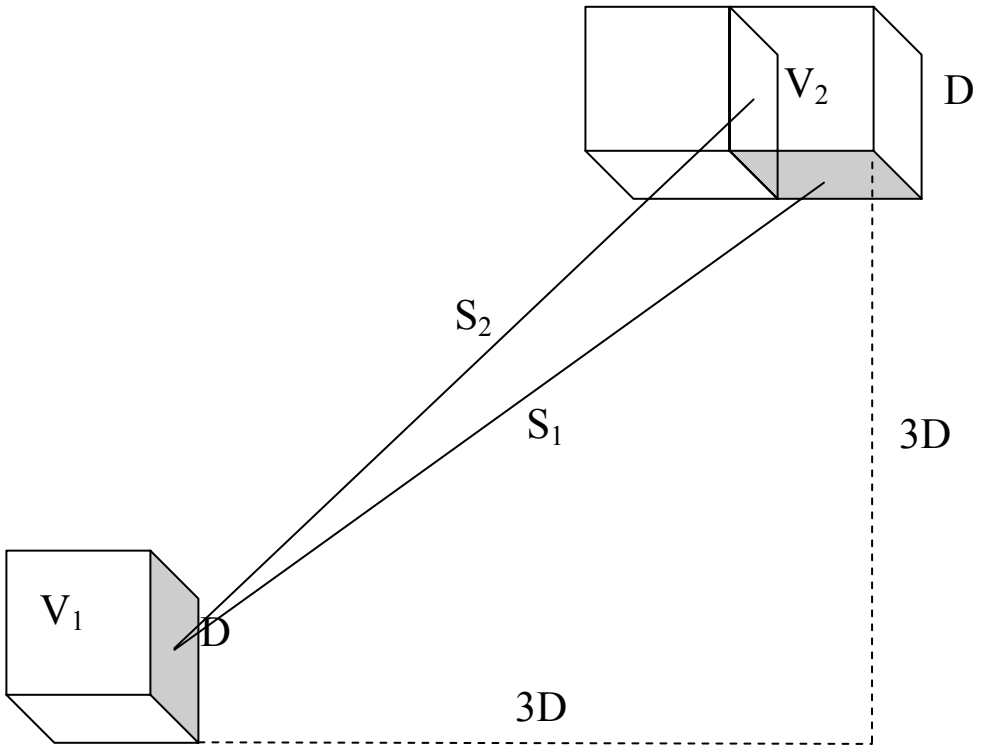

Figure 3: Example geometry highlighting the difference in "average absorption coefficient" for different optical path.

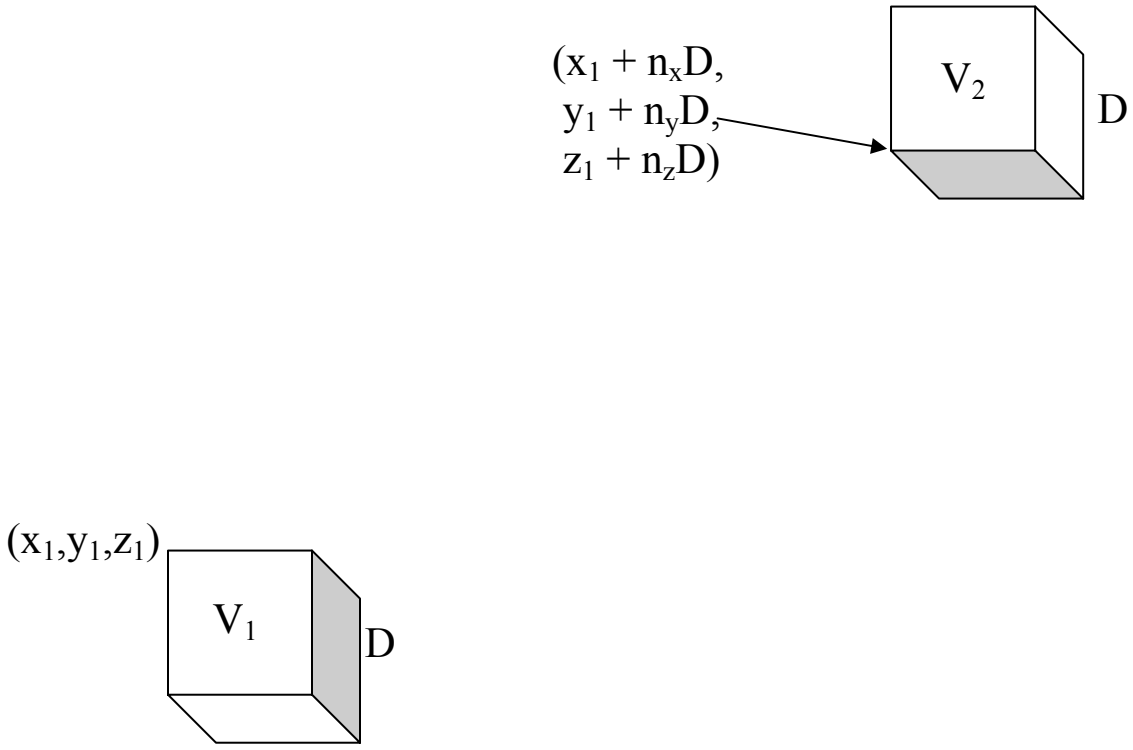

Figure 4: Geometry and coordinate system used in the definition of the g_1g_2 GEF.

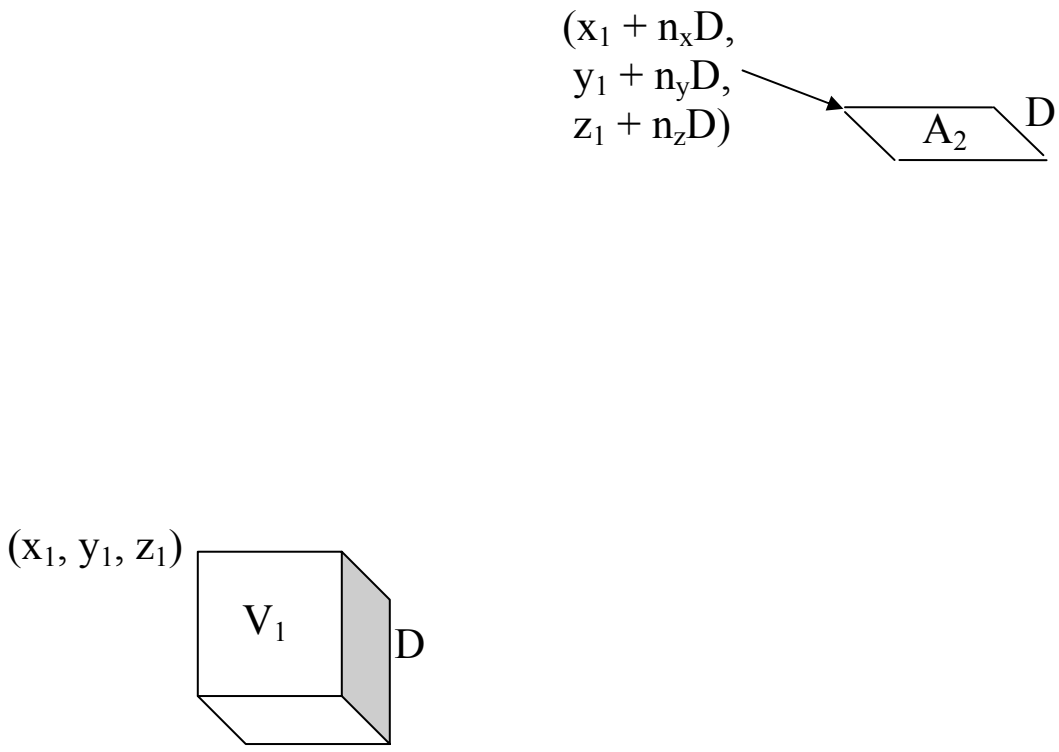

Figure 5: Geometry and coordinate system used in the definition of the $g_1 s_2$ GEF.

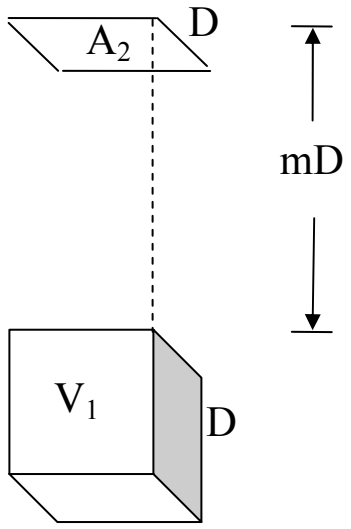

Figure 6: Geometry and coordinate system used in the illustration of the accuracy of the superposition procedure for the evaluation of the exchange factor $g_1 s_2$.

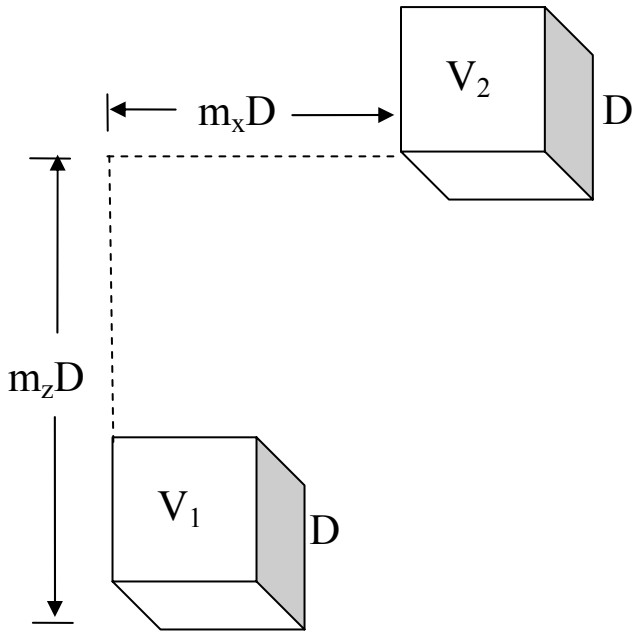

Figure 7: Geometry and coordinate system used in the illustration of the accuracy of the superposition procedure for the evaluation of the exchange factor $g_1 g_2$.

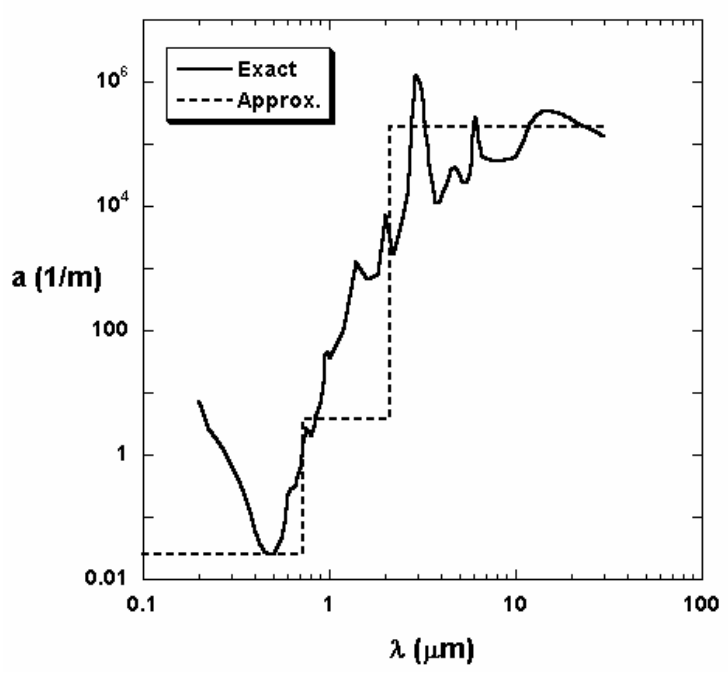

Figure 8: The 3-band approximation of the water absorption coefficient used in the premixing calculation.

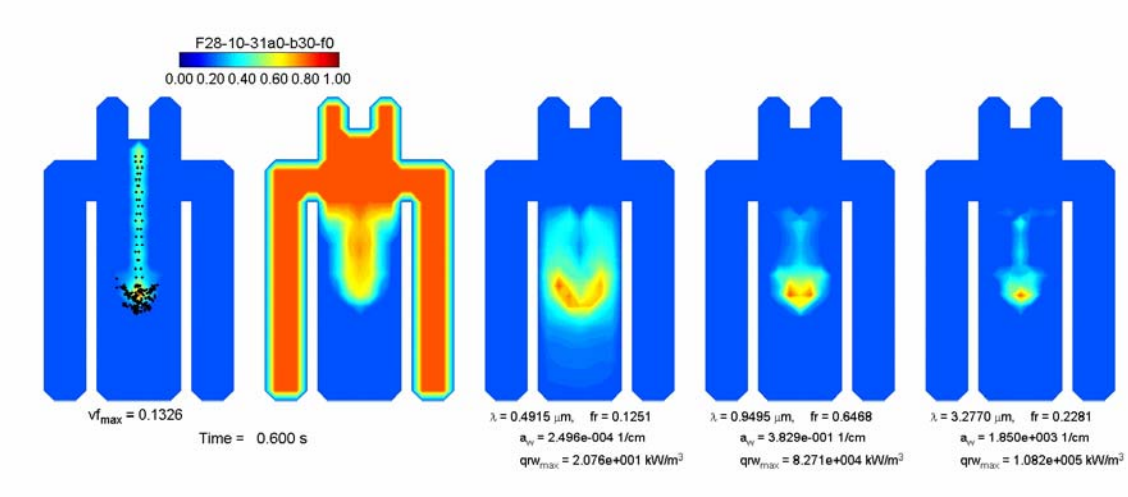

Figure 9a: The distribution of radiative absorption by water in the three absorption band (the right three figures) at 0.6 s after the initial pour predicted by the premixing calculation. The first figure on the left represents the distribution of the molten fuel (the black dots are the lagrangian particles representing fuel) and the second figure represents the void fraction distribution.

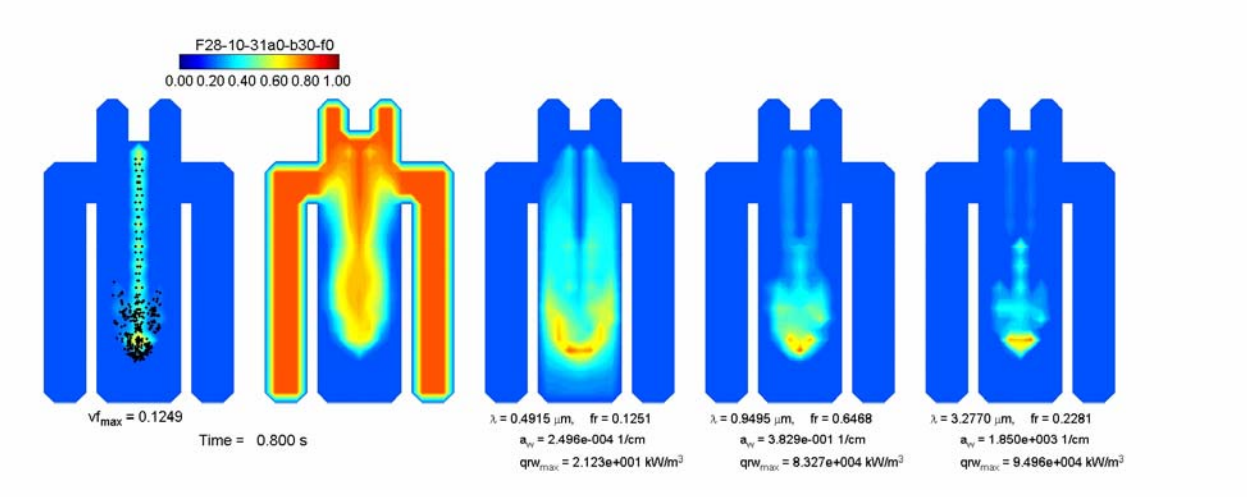

Figure 9b: The distribution of radiative absorption by water in the three absorption band (the right three figures) at 0.8 s after the initial pour predicted by the premixing calculation. The first figure on the left represents the distribution of the molten fuel (the black dots are the lagrangian particles representing fuel) and the second figure represents the void fraction distribution.

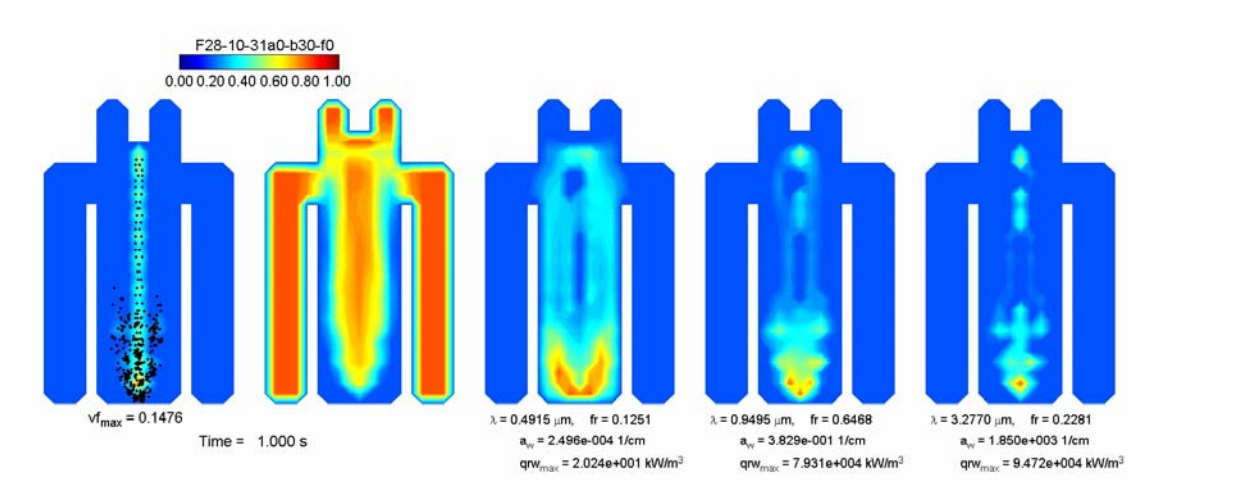

Figure 9c: The distribution of radiative absorption by water in the three absorption band (the right three figures) at 1.0 s after the initial pour predicted by the premixing calculation. The first figure on the left represents the distribution of the molten fuel (the black dots are the lagrangian particles representing fuel) and the second figure represents the void fraction distribution.